Multiscale Spatiotemporal Structures in Mode-Locked Fiber Lasers

Hani J. Kbashi[1], Marina Zajnulina[1], Amos G. Martinez[1], Sergey V. Sergeyev[1]

[1]School of Engineering and Applied Science, Aston University, Aston Triangle, Birmingham, B4 7ET, UK.
E-mails: m.zajnulina@aston.ac.uk , h.kbashi@aston.ac.uk

Received xxxxxx
Accepted for publication xxxxxx
Published xxxxxx

Abstract

Using an Er-doped fiber laser as a test bed, here we for the first time experimentally demonstrate the simultaneous effect of the fast scale (round-trip time) and slow scale (thousands round-trip time) instabilities on the emergence of breathers similar to the Akhmediev breathers, Peregrine solitons, and partially mode-locked chaotic solitons. The anomalous statistics of the laser output power justifies the connection of the observed spatiotemporal structures with bright and dark rogue waves. Apart from the interest in laser physics for revealing mechanisms of the multiscale dynamics, the obtained results can be of fundamental interest for studying spatiotemporal patterns induced by the interplay of the mechanisms mentioned above in various distributed systems.

Keywords: Mode-locked fiber laser, soliton rain, rogue wave, instabilities and chaos.

1. Introduction

For many decades, the universal nature of spatial and temporal patterns in fluids, granular media, plasma, nonlinear optics, and lasers have attracted researchers' attention [1-17]. For example, theoretical and experimental studies of various types of breathers or so-called "solitons on finite background" (SFBs) in the form of Akhmediev breathers (ABs), bi-periodic Akhmediev breathers (BPABs), and Peregrine solitons - spatially localized and temporally periodic structures on a finite background – play a crucial role in nonlinear science [1-8]. The SFBs constitute an analytic solution of the Focusing Nonlinear Schrödinger Equation (NLSE), the central model of waveguide and laser optics, hydrodynamics, plasma physics, and molecular biology [7-9]. In optics, ordinary ABs, BPABs and PSs arise due to the break-up of a slightly modulated continuous-wave (CW) optical field into a train of temporally periodic, but spatially localized pulses (ABs, [6]); train of temporally periodic and the spatially localized pair of pulses (BPABs, [4]); and single pulse with localization in time and space (PS, [5, 6]). This break-up is caused by modulation instability (MI) [1-9]. In the optical spectrum, the impact of MI manifests itself in the generation of a parametric cascade of spectral sidebands [3]. The MI seeded from noise, however, gives rise to the so-called rogue waves (RWs) [6]. The anomalous RWs' statistics implies more frequent events emergence as compared to the Gaussian or Rayleigh distributions. The amplitudes of these events are more than twice as large as the significant wave height (SWH) - the mean amplitude of the highest third part of the waves [10, 11]. At present, the SWH is defined as four times the standard deviation of the amplitude fluctuations [10]. Second mechanism for RW formation is the breather collision [5, 6].

It has been recently shown that not only MI can lead to the formation of spatiotemporal structures in an optical system, but also the so-called vector-resonance-multimode instability (VRMI) [12, 13]. The VRMI gives birth to spatiotemporal structures based on the growth of additional satellite frequencies in the spectrum of a mode-locked laser which results from the spatial modulation of the intra-cavity state of polarization (SOP) due to the increase of the birefringence strength caused by tuning the polarization controller [12, 13]. Additionally to the noise-driven and breather-collision-based generation of RWs, the VRMI is also able to give rise to the formation of optical RWs as reported in Ref. [13]. In addition to VRMI-based scenario of RWs emergence, RWs formation

driven by polarization instability leading to the desynchronization of the orthogonal SOPs was recently demonstrated experimentally and theoretically [14, 15].

Using an Erbium-doped fiber laser mode-locked with Carbon nanotubes as a test-bed, we for the first time demonstrate experimentally the formation of the fast-slow scale spatiotemporal structures based on a simultaneous effect of the soliton bunching [16], VRMI [12, 13] and polarization instability (PI) [14, 15]. Depending on the input power and the intra-cavity SOP, we observe the formation of breather structures similar to the fundamental ABs, PS, BPABs, and partially mode-locked chaotic solitons (CS). The evaluation of the laser output power statistics reveals the connection of the observed spatiotemporal structures with bright and dark RWs.

In detail, we observe the formation of fast-timescale AB-like structure due to the pulse bunching based on optoacoustic effects [16]. This structure reoccurs on the slow timescale every 500 roundtrips due to the phase difference slip between polarization states [13-15]. This phase slip gives rise to bright and dark RWs [15]. Increasing of the input power leads to the formation of structures similar to PS. Again, it arises due to the optoacoustic effects on the fast-time scale and the phase difference slip between the polarization states on the low timescale. The latter causes the emergence of bright RW. Further increase of the pump power results in the formation of bi-periodic AB-like structures. As in the case of AB-like structures, the bi-periodic ones arise due to the pulse bunching based on the optoacoustic effects on the fast-timescale and due to the VRMI effect on the slow timescale [12, 13]. The appearance of the bright RW associated with the bi-periodic ABs also occurs due to VRMI and not due to the polarization state phase slip as in previous cases. If the intra-cavity polarization state is changed, there arise partially mode-locked solitons that undergo the impact of the VRMI leading to their chaotic behavior. Also, the VRMI induces the formation of the bright RWs associated with chaotic solitons.

2. The Experimental Setup

The passively mode-locked fiber laser we use to observe various types of spatiotemporal structures is shown in Fig. 1. The laser cavity consists of a single-mode fiber (SMF) with a length of 7.6 m and 1.1 m long Erbium-doped fiber (EDF) pumped by a laser diode at 980 nm. The group-velocity dispersion parameters at 1550 nm are β_2^{SMF}=-22 ps^2/km and β_2^{EDF}=+59 ps^2/km resulting in the anomalous cavity net dispersion of β_2^{Net}=-11.76 ps^2/km. The lasing threshold occurs at the pump power of 14 mW. Passive mode locking is realized by a carbon nanotube saturable absorber (CNT) (cf. [13, 15]). The fundamental frequency of the mode-locked operation is 30 MHz. The polarization controllers POCs tune the birefringence of the laser cavity: POC2 is used to change the intra-cavity SOP, whereas POC1 controls the pump laser diode SOP. A polarization insensitive isolator (ISO) with 51 dB attenuation is deployed to ensure unidirectional operation of the ring cavity. A standard 70:30 fused output coupler (OC) redirects 30% of the laser light for detection and analysis [13, 15]. The laser output radiation from the 30% coupler is detected using a 50 GHz fast photodetector (Finisar XPDV2320R) with 33 GHz bandwidth. The output photodetector voltage is recorded by an 80 GSa/s sampling rate oscilloscope (Agilent DSOX93204A). The recorded oscilloscope traces have a length of 26 ms with the effective resolution of 12.5 ps per point. To visualize and analyze the laser

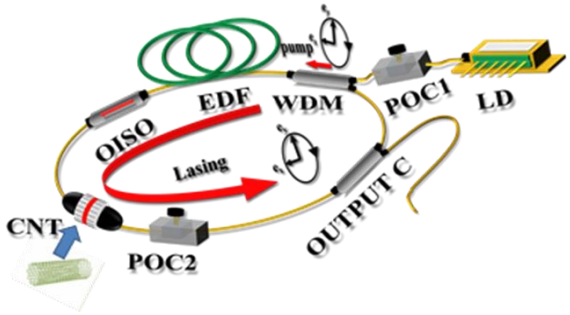

Fig. 1. The Experimental setup.. WDM - wavelength Division multiplexing; PC - polarization controller; OISO - optical isolator; SA: CNT - saturable absorber with carbon nanotubes; and OUTPUT C: output coupler.

field intensity, we split these 26 ms oscilloscope traces into segments that coincide with the cavity roundtrip time and then stack them into a matrix of 5000 roundtrips. Plotting this matrix as a 3D diagram gives us the possibility to study the formation of the spatiotemporal structures of the laser field as a function of the cavity roundtrip time and the number of cavity roundtrips. Additionally, we characterize the observed laser regimes using a radio-frequency (RF) spectrum analyzer (Rohde and Schwarz, 10 Hz − 13.6 GHz) [13, 15]. The resolution used in the RF and optical spectrum measurements is 3 Hz and 0.02 nm, respectively. To get insight into the mechanism of the emergence of the spatiotemporal structure at the slow time scales of 1 μs – 20 ms (30 round-trips), we used a polarimeter (IPM5300, Thorlabs) to record the normalized Stokes parameters s_1, s_2, s_3. Those are related to the output powers of two linearly cross-polarized SOPs, I_x and I_y, and to the phase difference between them $\Delta\phi$ [13-15]

$$S_0 = I_x + I_y, \quad S_1 = I_x - I_y, \quad S_2 = 2\sqrt{I_x I_y}\cos\phi, \; S_3 = 2\sqrt{I_x I_y}\sin\phi, \; s_i = \frac{S_i}{\sqrt{S_1^2+S_2^2+S_3^2}}, \; (i = 1,2,3) \quad (1)$$

To be able to make statements about the presence of RWs in the system, we plot distribution histograms of the photodetector voltage normalized as follows: $V_n = \frac{(V-\text{median}\,(V))}{\sigma(V)}$. In these histograms,

bright RWs appear for $V_n > 8$, whereas the dark ones for $V_n < -8$ [13, 15].

In general, the mode-locked laser, as shown in Fig. 1 operates in three different regimes: CW, the formation of various spatiotemporal structures similar to the fundamental and second-order ABs, PS, and partial and stable mode-locking. In the following, we exclude the stable mode-locking and CW regime from consideration and focus only on the formation of spatiotemporal structures and partially mode-locked pulses.

3. Results and Discussion

Here, we present results on observation of various spatiotemporal structures in the laser (Fig. 1) similar to the fundamental and second-order ABs, PS, and CS as well as their statistics satisfying the criteria of optical bright and/or dark RWs. We perform our studies starting with the pump power slightly above the laser threshold of 14 mW and increase it to 20 mW.

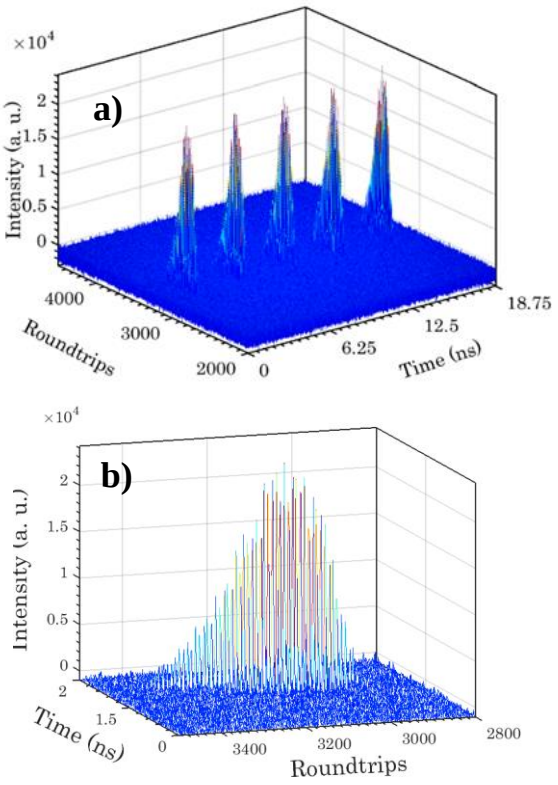

Fig. 2. Spatiotemporal structures similar to the Akhmediev breather observed at 16.3 mW: a) fast-timescale view, b) slow-timescale view.

The experimental results obtained for the pump power of 16.3 mW are shown in Fig. 2 (a, b). It depicts a train of pulses that are periodic in time but localized in space along the propagation distance (coinciding with the laser roundtrip number).

Unlike emergence of the AB that results from an MI-based break-up of a CW field [1, 3, 4-6, 8, 9], the pulse bunching

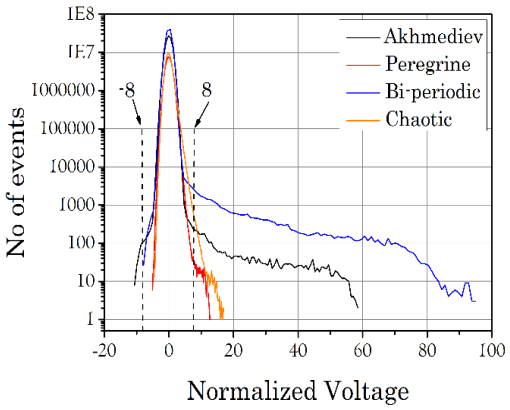

Fig. 3. Distribution of normalized photodetector voltage in case of spatiotemporal structures similar to Akhmediev breathers (black), Peregrine solitons (red), bi-periodic Akhmediev breathers (blue), and chaotic solitons (orange). Bright rogue waves appear for voltage $V_n > 8$, dark rogue waves for $V_n < -8$ [13, 14].

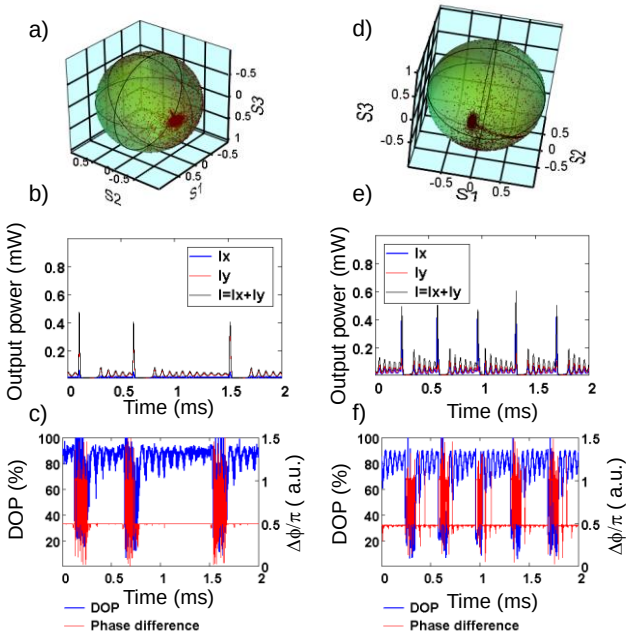

Fig. 4. Polarization laser dynamics of spatiotemporal structures similar to the Akhmediev breathers (a-c) and Peregrine solitons (d-f) at the time scale of thousands of round trips (1 μs resolution, i.e. averaging over approximately 33 round trips). a), d) trajectories on normalized Poincaré sphere; b), e) the output powers vs time; c), f) Degree of polarization and the phase difference vs time. Pump power: a) – c) 16.3 mW, d) - f) 18 mW.

with the period of 3.84 ns is caused by long-range solitons interaction that arises from optoacoustic effects and dispersive wave perturbations [16]. The AB-like spatiotemporal structure reoccurs on the slow-timescale with periodicity of 500 roundtrips. The reoccurrence arises due to the phase difference slip between the polarization states (Fig. 4.b). The evaluation of the normalized photodetector voltage representing the

intensity of the breather pulses reveals a skewed distribution

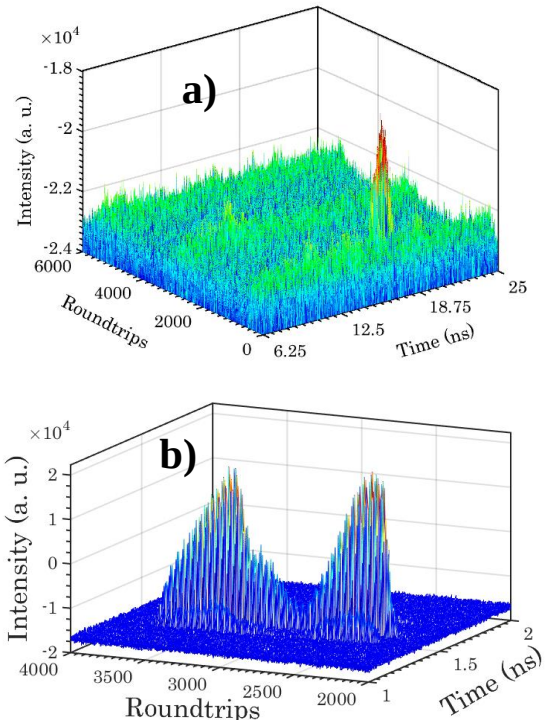

Fig. 5. Spatiotemporal structures similar to the Peregrine soliton observed at 18 mW: a) fast-timescale view, b) slow- timescale view.

(Fig. 3, black). The long right-hand-side tail of this distribution exceeds the value of 8 denoting the existence of bright RWs associated with the observed AB. The left-hand-side tail of the distribution trespasses the value of time scale of 1 ms – 15 ms (Fig. 4 (a-c)), the dynamics is mostly localized nearby linear-polarized SOP whereas formation of bright RWs occurs due to the phase difference slip in π between this SOP and the orthogonal one (Fig. 4 (a, c)). As shown in our previous publications [13-15], this phase slip is driven by the orthogonal SOPs' desynchronization leading to the emergence of irregular AB-like spikes taking the form of bright RWs.

The increase of the pump power to 18 mW gives rise to the appearance of spatiotemporal structures similar to PS in the context of single-pulse localization at the round trip and periodicity of 1000 roundtrips (Fig. 5 (b)). Again, the structures arise due to the optoacoustic effects on the fast timescale and reappears every 1000 roundtrips due to the phase difference slip between the polarization states on the slow timescale. As seen in Fig. 3 (red), the condition for the normalized voltage $V_n > |8|$ for the RWs to exist is only fulfilled for bright RWs in the case of the PS. The same as for ABs-like structures, the appearance of RWs is supported by the phase difference slip between the orthogonal SOPs (Fig. 4 d-f)). $V_n = -8$ indicating the existence of dark RWs (cf. [10, 11, 13-15]).

At pump power of 20 mW, the laser starts emitting pulses that are periodic in time and space (therefore also called BPABs-like structures in the scope of this paper) (Fig. 6 (a, b)). These bi-periodic pulses with the temporal periodicity of

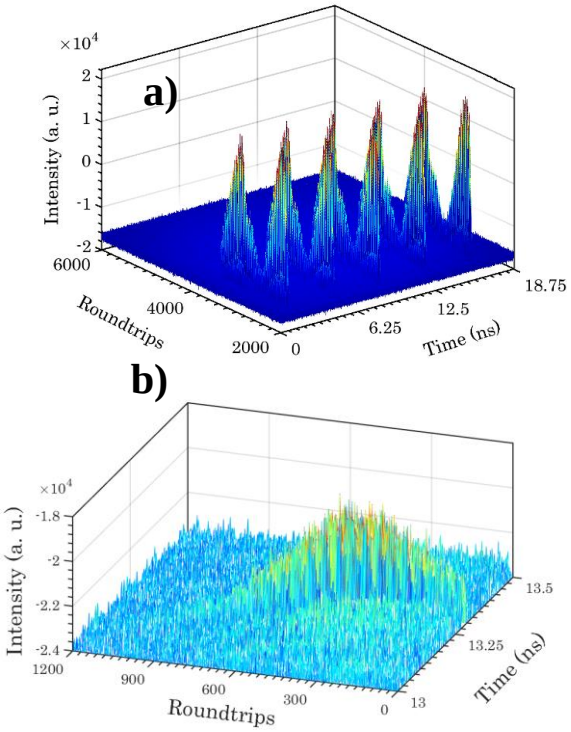

Fig. 6 Spatiotemporal structures similar to the bi-periodic (second-order) Akhmediev breather observed at 20 mW: a) fast-timescale view, b) slow- timescale view.

3.84 ns constitute an overlap of two Akhmediev breathers-like structures [7]. The same for the case shown in Fig.2, the fast-timescale pulse bunching with the period of 3.84 ns (Fig. 6 (a)) is driven by optoacoustic effects and dispersive wave perturbations [16]. The BPABs-like structures reoccur with the periodicity of 330 roundtrips as shown in Fig. 6 (b). Unlike in the previous cases, this reoccurrence takes place due to the spatial modulation of the optical field, and not due to the phase

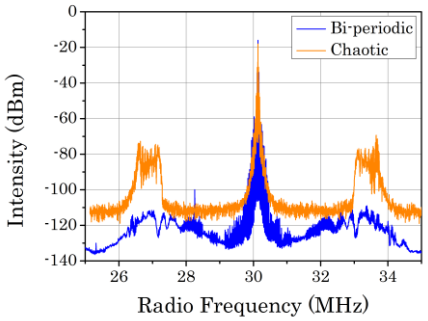

Fig. 7. Radio frequency spectra of the observed bi-periodic-(second-order) Akhmediev breather-like structures (blue) and chaotic solitons (orange).

difference slip between the polarization states. This spatial modulation is caused by the VRMI [12, 13]. The VRMI occurs due to the increased intra-cavity birefringence and results in the appearance of satellite lines in the RF spectrum (Fig. 7, blue). In the case of the mismatch between the satellite and

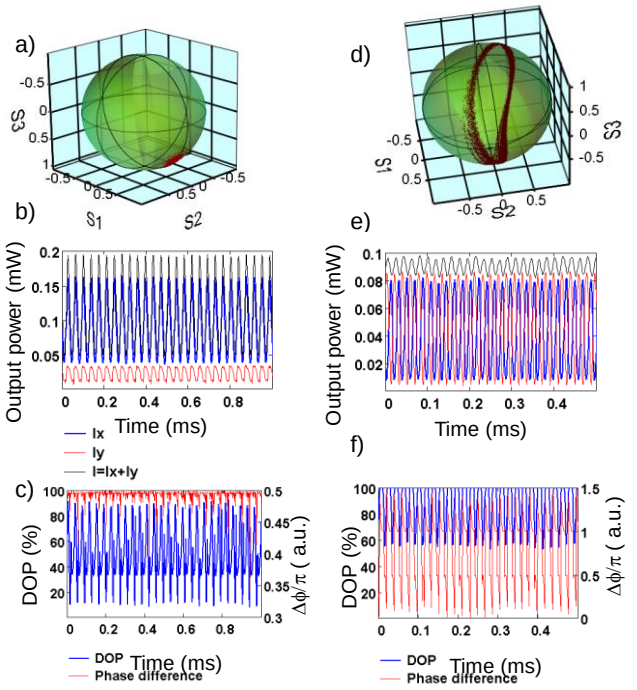

Fig. 8 Polarization laser dynamics of spatiotemporal structures similar to the bi-periodic (second-order) Akhmediev breathers (a-c) and chaotic solitons (d-f) at the time scale of thousands of round trips (1 μs resolution, i.e. averaging over approximately 33 round trips). a), d) trajectories on normalized Poincaré sphere; b), e) the output powers vs time; c), f) Degree of polarization and the phase difference vs time. Pump power: a) – c) 18 mW, d) – f) 20 mW.

adjacent harmonic frequencies, the rational relation between frequencies can be realized such that it enables quasi-periodic motion (torus in the phase space) and so the emergence of the chaotic behavior through the Ruelle-Takens-Newhouse scenario (route to chaos via the two-dimensional torus destruction [17]). The mechanism of RW emergence is related to the fast-scale chaotic behavior based on VRMI rather than the phase difference slip at thousands round trips scale. The fast dynamics-based RW emergence scenario is confirmed by the localization of the SOP, slow regular oscillations of the output power and degree of polarization (DOP) decreasing at slow-timescale (Fig. 8 (a-c)). The polarimeter resolution of 1 μs shows dynamics averaged over approximately over 30 round trips (Fig. 8). As follows from Fig. 8 (a), averaged trajectories are localized in a small spot, whereas the real trajectories are located in a larger area. If Stokes parameters change sign, then the DOP decreases as follows from the Eqs.1. Thus, the polarization dynamics is evolving slowly for the cases shown in Figs. 4 and vice versa SOP is evolving fast for the cases shown in Figs. 8. The right-skewed distribution

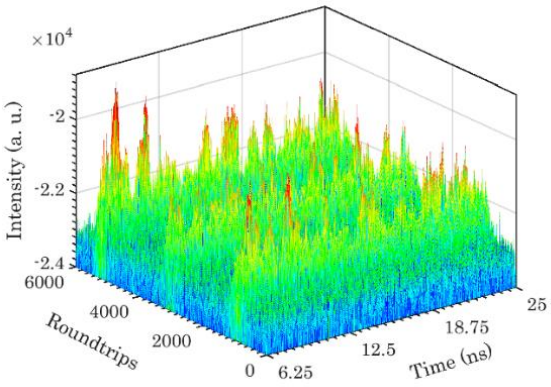

Fig. 9. Chaotic mode-locked solitons observed at the pump power of 20 mW.

of the bi-periodic ABs-like structures as shown in Fig. 4 (blue) gives rise to the association between these breathers and the second-order RWs (cf. [13, 15]). The value of the normalized voltage of $V_n < -8$ is however not trespassed. Accordingly, the condition for the dark RWs appearance is not fulfilled. So, there are no dark RWs in the case of a bi-periodic breather, only bright ones are present.

The change of the intra-cavity lasing SOP via tuning of the polarization controller POC2 at the same pump power of 20 mW results in the formation of chaotic pulses (Fig. 9). These pulses arise due to the partial passive mode-locking in the laser cavity. However, they undergo the impact of VRMI which manifests itself in broad frequency satellites around 27 MHz and 33 MHz of the RF spectrum (Fig. 7, orange). The same way as for the bi-periodic ABs, the rational relation between satellites and fundamental frequencies (9:10:11) enables quasiperiodic motion and so the emergence of the chaotic behavior and RWs through the Ruelle-Takens-Newhouse scenario [17]. The distribution of the normalized photodetector voltage (Fig. 5, orange) confirms the generation of bright RWs for the given value of the pump power and the state of polarization. The threshold for dark RWs of $V_n = -8$ is not achieved though meaning that there are no dark RW for the given set of parameters. Again, the RWs arise due to the impact of VRMI. Unlike the previous case of BPABs, the polarization dynamics with equal output powers for orthogonal SOPs (Fig 8 (e)) is slow that is confirmed by DOP values of 80 % and trajectory at the Poincare sphere (Fig. 8 (d, f)).

4. Summary

Using an Erbium-doped fiber laser mode-locked with carbon nanotubes [13, 15], we observe the formation of spatiotemporal structures similar to the fundamental and bi-periodic (second-order) Akhmediev breathers-, Peregrine solitons-like structures, and partially mode-locked chaotic solitons. These different kinds of structures arise depending on the laser input power and the intra-cavity state of polarization. For the first time, we demonstrate the formation

of spatiotemporal structures driven by a simultaneous effect of the soliton bunching and two instabilities, namely vector-resonance-multimode instability and the polarization instability leading to the orthogonal SOPs desynchronization. Specifically, we show that the soliton bunching at the fast-timescale and phase difference slip between orthogonal SOPs of the laser field (slow-timescale) induce the formation of bright and/or dark rogue waves in the case of fundamental and second-order Akhmediev breathers- and Peregrine solitons-like structures. In the case of second-order Akhmediev breathers-like structures and chaotic solitons, the vector-resonance-multimode instability leads to the chaotic behavior of the pulses through route to chaos via the two-dimensional torus destruction [17]). Unlike the previous cases of ABs- and PS-like structures, the mechanism of RW emergence is related to the fast-scale chaotic behavior based on VRMI rather than the phase difference slip at thousands round trips scale. Revealed mechanism of emergence of various optical spatiotemporal structures driven by vector-resonance-multimode instability and the SOPs desynchronization can complement existing mechanisms of spatiotemporal structures formation in various distributed systems. The demonstrated approach for the spatiotemporal patterns tunability based on the change of laser input power and the state of polarization can find potential applications for unlocking a variety of laser dynamics in the context of applications ranging from fiber optic communications to biomedicine.

Acknowledgments

The authors would like to thank Dr. Aleksey Rozhin for providing the carbon nanotubes for the saturable absorber. This work was supported by The Leverhulme Trust (Grant ref: RPG-2014-304) and the European Commission via H2020-MSCA-RISE-2018 HALT (Project ID 823937). Marina Zajnulina and Amos G. Martinez acknowledge the EC-funding from the H2020-MSCA-IF scheme (Project ID 792421 and Project ID 659222, respectively).

References

[1] Akhmediev N.N. & Korneev, V.I. 1986. *Theor. Math. Physics* **69**(2), 1089-1093.
[2] Kibler B., Fatome J., Finot C., Millot G., Genty G., Wetzel B., Akhmediev N., Dias F. & Dudley J.M. 2012. *Scientific reports* **2**, 463.
[3] Agrawal G., in Nonlinear Fiber Optics, 5th Edition (Academic Press, 2012).
[4] Hammani K., Wetzel B., Kibler B., Fatome J., Finot C., Millot G., Akhmediev N. & Dudley J.M. 2011. *Optics letters* **36**(11), 2140-2142.
[5] Kedziora D.J., Ankiewicz A. & Akhmediev N. 2012. *Physical Review E* **85**(6), 066601.
[6] Dudley J.M., Dias F., Erkintalo M. & Genty G., 2014 *Nature Photonics* **8**(10), 755.
[7] Kibler B., Fatome J., Finot C., Millot G., Dias F., Genty G., Akhmediev N. & Dudley J.M. 2010. *Nature Physics* **6**(10), 790.
[8] Akhmediev, N. & Ankiewicz, A. Solitons: Non-linear Pulses and Beams (Chapman & Hall, 1997).
[9] Chin S.A., Ashour O.A. & Belić M.R., 2015 *Physical Review E* **92**(6), 063202.
[10] Onorato M., Residori S., Bortolozzo U., Montina A. & Arecchi F.T. 2013 *Physics Reports* **528**(2), 47-89.
[11] Lecaplain C., Grelu P., Soto-Crespo J.M. and Akhmediev, N. 2012. *Physical review letters* **108**(23), 233901.
[12] Sergeyev S.V., Kbashi H., Tarasov N., Loiko,Y. & Kolpakov S.A. 2017. *Physical review letters* **118**(3), 033904.
[13] Sergeyev S. V., Kbashi H., Mou, C. Martinez A., Kolpakov S, Kalashnikov V., in book Chapter 9 (IOP Publishing, 2018) p. 9-01 - 9-24.
[14] Sergeyev S.V. 2016. *Optics letters* **41**(20), 4700-4703.
[15] Kbashi H, Sergeyev S.V, Mou C, Garcia A.M, Araimi M.A, Rozhin A, Kolpakov S and Kalashnikov V 2018 *Annalen der Physik*, **530**, 1700362.
[16] He W., Pang M., Yeh D.H., Huang J., Menyuk C.R. & Russell P.S.J., 2018. Non-covalent bonds between optical solitons in an optoacoustically mode-locked fiber laser: Analysis & modelling. arXiv preprint arXiv:1808.00824.
[17] Anishchenko V.S., Astakhov V., Neiman A., Vadivasova T. & Schimansky-Geier, L. Nonlinear dynamics of chaotic and stochastic systems: tutorial and modern developments. (Springer Science, 2007), p. 121.